LIMNOLOGY and OCEANOGRAPHY

ASLO

Limnol. Oceanogr. 9999, 2023, 1–14

doi: 10.1002/lno.12295

Spatial and temporal drivers of fluorescence quantum yield variability in the Southern Ocean

Thomas James Ryan-Keogh,[1*] **Emma Lewis Bone**,[1,2,3,4] **Sandy J. Thomalla**,[1,2] **Lisl Lain**,[3] **Marie E. Smith**,[3,5] **Stewart Bernard**,[6] **Marcello Vichi**[2]

[1]Southern Ocean Carbon-Climate Observatory, CSIR, Cape Town, South Africa
[2]Marine and Antarctic Research Centre for Innovation and Sustainability, University of Cape Town, Cape Town, South Africa
[3]Coastal Systems and Earth Observation Research Group, CSIR, Cape Town, South Africa
[4]Nansen-Tutu Centre for Marine Environmental Research, University of Cape Town, Cape Town, South Africa
[5]Department of Oceanography, University of Cape Town, Cape Town, South Africa
[6]South African National Space Agency, Cape Town, South Africa

Abstract

Fluorescence quantum yield is a powerful tool for assessing phytoplankton photophysiology and photosynthetic efficiency, but there is a paucity of in situ studies. Here we present the first wavelength-specific fluorescence quantum yield data from high spatial and temporal resolution real-time measurements made in the Southern Ocean. This dataset represents both winter and summer conditions across a broad latitudinal range of the Atlantic and Indian South Ocean and the presented analysis assesses the potential influence of a range of physical, chemical, and biological drivers of variability. The results indicate that both light history and potential iron limitation play significant roles in constraining the magnitude of fluorescence quantum yield on a seasonal basis, with links to specific pigment composition of carotenoids involved in fluorescence quenching. Whereas community structure and associated pigment content play a strong role in dictating the spectral shape of fluorescence quantum yield both seasonally and spatially, with larger diatom-dominated communities fluorescing more in the blue region of the spectrum and smaller phycoerythrin-containing phytoplankton fluorescing more in the green-orange region of the spectrum. This study provides a better understanding of the drivers of variability of in situ fluorescence quantum yield, which is useful for informing interpretations of studies based on remotely sensed signals, which are essential for investigating spatial and temporal variability in photophysiological characteristics on longer time scales.

The use of natural, or sun-induced chlorophyll *a* (Chl *a*) fluorescence (SICF) as an indicator of phytoplankton photophysiological status requires knowledge of the fluorescence quantum yield (Φ) and the factors that control its variability (Babin et al. 1996; Letelier et al. 1997; Maritorena et al. 2000; Abbott et al. 2001; Morrison 2003; Westberry and Siegel 2003; Schallenberg et al. 2008; Behrenfeld et al. 2009; Westberry et al. 2013; Browning et al. 2014; Lin et al. 2016). In situ Φ_F is defined as the ratio of photons emitted as fluorescence to those absorbed by phytoplankton and is referred to as an apparent Φ_F. Variability in Φ_F is due to changes in energy distribution within the photosynthetic apparatus resulting from modifications to light absorption and fluorescence emission in each cell. These modifications are expressed as physiological responses to varying environmental conditions with adaptive features that can be attributed to three principal drivers namely the light environment, nutrient availability, and community structure.

Any interpretation of Chl *a* fluorescence under varying ambient light conditions requires an understanding of the adjustments in photochemical quenching (qP) and non-photochemical quenching (qN) of Chl *a* fluorescence. Photochemical quenching occurs at low irradiance levels and decreases as light levels increase, with reaction centers progressively closing (Kiefer and Reynolds 1992). Under high light

*Correspondence: tryankeogh@csir.co.za

Additional Supporting Information may be found in the online version of this article.

Author Contribution Statement: The study was conceptualized by S.J.T. and S.B. Data collection was performed by E.L.B., S.J.T., and M.E.S. Data were prepared by T.J.R.K., E.L.B., and M.E.S., and all authors contributed to the analysis. T.J.R.K. prepared the manuscript, and all authors approved the final version.

conditions, qN acts to regulate exciton energy transfer to Photosystem II (PSII) reaction centers by balancing photochemical utilization and excess energy dissipation through antenna quenching (qE) and reaction center quenching (qI) (Krause and Weis 1991; Müller et al. 2001; Horton and Ruban 2005). qE is a rapid (seconds to minutes), energy-dependent mechanism that typically dissipates excess energy through the xanthophyll cycle (XC) (Demmig-Adams 1990; Lavaud et al. 2002). The XC in phytoplankton (e.g., in diatoms, haptophytes, and dinoflagellates) mediates the interconversion of diadinoxanthin (Dd) and diatoxanthin (Dt) in response to changing light conditions (Demers et al. 1991), or it involves the conversion of violaxanthin into zeaxanthin via the intermediate antheraxanthin (e.g., in chlorophytes and chrysophytes) (Brunet et al. 2011). Implementation of qI occurs over a longer timescale, through the reversible down-regulation of PSII reaction centers (Morrison 2003). Under high irradiance levels Φ is typically low, due to qN, and under low light conditions Φ is typically high, subject to qP (Maritorena et al. 2000; Morrison 2003; Westberry and Siegel 2003; Laney et al. 2005; Schallenberg et al. 2008; Behrenfeld et al. 2009; Morrison and Goodwin 2010; Ostrowska 2012). In addition to qN, the photoacclimation state of phytoplankton to their ambient surroundings must be considered when investigating the light response of a population. Beyond light, both community structure and nutrient availability also play a strong role in driving Φ_F variability. For example, any phytoplankton that employ the xanthophyll cycle will have reduced Φ_F under high light conditions (Kropuenske et al. 2009), which includes both diatoms (Lavaud et al. 2002) and *Phaeocystis antarctica* (Moisan and Olaizola 1998). Although ΦF can be influenced by macronutrient (nitrate, phosphate, silicate) limitation, for example, under phosphate limitation phytoplankton cells are unable to carry out photosystem repairs (Wykoff et al. 1998), Φ_F is typically considered a poor proxy for macronutrient limitation when investigated with SICF (Schallenberg et al. 2008). On the other hand, limitation by the micronutrient iron, a vital element required for photosynthetic electron transport (Raven et al. 1999), is known to drive an increase in Φ_F (Lin et al. 2016). This is due to a decrease in the number of functional reaction centers and an increase in the pool of light harvesting complexes (Strzepek et al. 2019), some of which may be energetically uncoupled (Greene et al. 1991; Schrader et al. 2011; Macey et al. 2014). At low light, these large light harvesting complexes increase energy loss through both thermal dissipation and fluorescence (Wientjes et al. 2013), whereas at high light the remaining functional reaction centers are subject to overexcitation and increases in qN.

The derivation of Φ_F requires, besides accurate quantification of the fluorescence signal, knowledge of the spectral absorption capacity of phytoplankton and a fully characterized light field. Field studies of Φ_F typically involve SICF measurements (Letelier et al. 1997; Maritorena et al. 2000; Morrison 2003; Schallenberg et al. 2008) or proxies derived from active fluorometry (Browning et al. 2014; Lin et al. 2016); however, the use of multiexcitation fluorometers in the derivation of Φ_F has been proposed (Ostrowska 2012; Griffith et al. 2018). Multiexcitation fluorometers typically exploit fluorescence excitation spectra to define phytoplankton taxonomic groups based on signature accessory pigment composition (Sosik and Mitchell 1995; Johnsen et al. 1997), which is used to discriminate between phytoplankton species in mixed assemblages (Cowles et al. 1993; Beutler et al. 1998, 2002, 2003). For example, Yoshida et al. (2011) demonstrated that a Multi-Exciter Fluorometer (MFL, JFE Advantech Co., Ltd.) could measure the excitation spectra of a water sample and differentiate between three phytoplankton groups (diatoms, green algae and cyanobacteria) for the monitoring of harmful algal blooms. However, a study by Ostrowska (2012) further utilized a BBE Moldaenke FluoroProbe multi-excitation fluorometer to derive wavelength-specific Φ_F. Although they did not radiometrically characterize the excitation light-emitting diodes (LEDs) nor the emission detector of the instrument, they were still able to infer apparent, wavelength-specific Φ_F values. More recently, Griffith et al. (2018) employed a MFL to derive fully characterized absolute measurements of wavelength-specific Φ_F. The advantages of wavelength-specific Φ_F over measurements centered around the peak absorption of Chl *a* is that it allows us to determine the importance of pigments that span a large range of the absorption spectra, which includes both photoprotective and photosynthetic carotenoids, under different environmental conditions.

The aim of this study was to deploy the MFL in the field to derive absolute Φ_F (λ) measurements in the Atlantic Southern Ocean in austral winter (2012) and summer (2013/2014) to address the hypothesis that seasonality would be the dominant driver in Φ_F (λ). The calibration factors derived by Griffith et al. (2018) were used together with underway (UW) real-time measurements of MFL-fluorescence and phytoplankton specific absorption measurements to calculate absolute Φ_F (λ) values. Spectral analysis was performed on all derived Φ_F (λ) such that potential relationships between Φ_F (λ) and possible drivers of variability could be established.

Materials and methods

Cruises

The data presented here were obtained from two cruises carried out on-board the S.A. Agulhas II, in the Atlantic and Indian sectors of the Southern Ocean (Fig. 1). The first cruise was during the austral winter of 2012 (Fig. 1a; Winter 12, 09 July 2012 to 01 August 2012) and the second was in the austral summer of 2013/2014, as part of the South African National Antarctic Expedition 53 (Fig. 1b; SANAE 53, 28 November 2013 to 13 February 2014), hereafter referred to as the winter and summer cruises. Samples for seawater

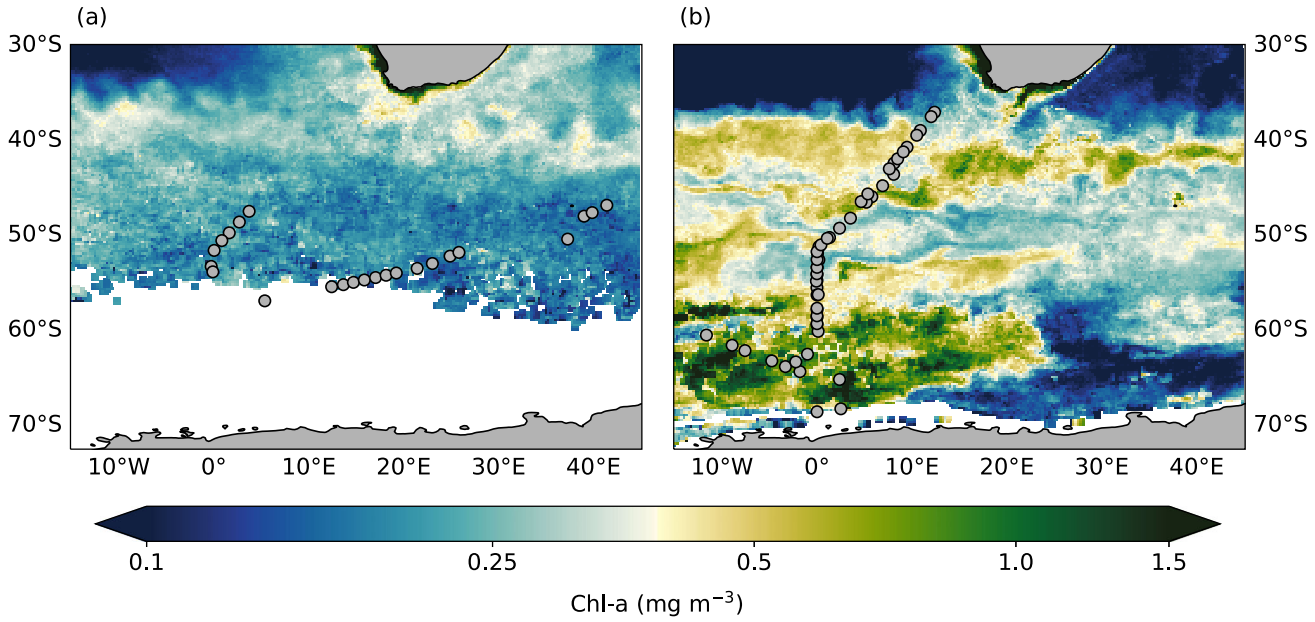

Fig. 1. Composite maps of satellite-derived Chl *a* (mg m^{-3}) showing locations of Φ_F measurements during (**a**) winter (July 2012 to August 2012) and (**b**) summer (December 2013 to February 2014). Satellite Chl *a* data were obtained from the ocean color climate change initiative (Sathyendranath et al., 2019; v5.0).

analysis were collected from the UW scientific seawater supply every 2–4 h hereafter referred to as an UW station.

Fluorescence measurements

Fluorescence was measured with an MFL, which comprises nine excitation LEDs (375, 400, 420, 435, 470, 505, 525, 570, and 590 nm) and detects emitted light between 640 and 1000 nm. The MFL was oriented with the optical window facing down in a nonfluorescent, black perspex bucket, with light-excluding inflow and outflow tubing, at a distance $z \approx 60$ mm from the bottom. The bucket was connected to a continuous supply of the ship's UW scientific seawater, the intake of which was approximately 7 m below the sea surface. The seawater supply was passed through a debubbler to reduce the intake of bubbles. Fluorescence measurements were continuously recorded for 10 s every 1 min and were averaged into 20 min bins (UW station ± 10 min) during processing, to capture the same population present in overlapping station measurements that included phytoplankton absorbance (a_{ph}) and high-performance liquid chromatography (HPLC). These bins incorporate upper and lower limits (mean ± standard deviation × 3) to exclude outliers.

Further manual inspection allowed for the exclusion of data with bubbles evident by high turbidity values. The 880-nm MFL waveband was used as a flag for highly scattering environments and proved to be significantly related to the 570-nm waveband fluorescence output ($p < 0.001$, data not shown). The validity of the MFL calibration models described by Griffith et al. (2018) is contingent upon deployment in a low scattering environment such that fluorescence samples considered to be contaminated with scattering elements were excluded, that is, those stations with a turbidity value greater than 8 Formazine Turbidity Units. Φ_F (λ) were subsequently derived for each MFL excitation wavelength using wavelength-specific fluorescence, spectrally averaged a_{ph} (see "Light history" section) and the MFL calibration coefficients from Griffith et al. (2018) as described below in Eq. 1:

$$\Phi_F(\lambda) = \frac{R(\lambda)}{k(\lambda) a_{ph} P_c}, \quad (1)$$

where $R(\lambda)$ is the MFL signal response at each wavelength, $k(\lambda)$ is the calibration constant from the ATTO 490LS dye (*see* Griffith et al. 2018 for more details), aph (λ) is the wavelength specific phytoplankton absorption normalized to the spectra of the MFL-LED (λ), and P_c is the MFL-relative partial quantum yield factor comprised of the mean values of Chl *a* in ether and methanol ($P_c = 0.851$). As the MFL filters out part of the dye emission it is necessary to calculate the relative partial quantum yield, which lies between 0 and 1 and takes into account the spectral response of the MFL detector channel.

High-performance liquid chromatography

Pigment samples were collected every 2–4 h by filtering ~ 2 L of seawater from the ship's scientific seawater supply through 0.7-μm Whatman GF/F (25 mm) filters under pressure of less than 10 mmHg. Filters were flash frozen in liquid nitrogen and stored at −80°C until HPLC analysis was conducted

at the Laboratoire d'Océanographie de Villefranche-sur-Mer (Villefranchesur-Mer, France). Samples were subjected to HPLC (Agilent Technologies 1200) following the methods of Ras et al. (2008); the limits of detection were on the order of 0.1 ng L^{-1}. All Chl *a* values used in this study constitute HPLC-derived total Chl *a* measurements (the sum of Chl *a*, divinyl-Chl *a*, and chlorophillide-a), apart from the total Chl *a* less divinyl-Chl *a* used in Chemical Taxonomy (CHEMTAX) analysis.

Chemical taxonomy

Pigment composition data were standardized through root square transformation before cluster analysis utilizing multidimensional scaling, where similar samples appear together, and dissimilar samples do not. Samples were grouped and analyzed through CHEMTAX (Mackey et al. 1996) using the Southern Ocean-specific pigment ratios from Gibberd et al. (2013). Multiple iterations of pigment ratios were used to reduce uncertainty in the taxonomic abundance as described in Gibberd et al. (2013), with the solution that had the smallest residual used for the estimated taxonomic abundance.

Phytoplankton size classes

Phytoplankton size classes, that is, picophytoplankton (0–2 μm), nanophytoplankton (2–20 μm), and microphytoplankton (20–200 μm), were estimated following the approach of Vidussi et al. (2001). Seven size class marker pigments, extracted by HPLC, were weighted as per Uitz et al. (2006), and used to estimate the size classes of phytoplankton in a mixed population.

Additional pigments

Pigment composition data were also used to calculate the amounts of photosynthetic and photoprotective carotenoids, where photosynthetic carotenoids (PSC) include peridin, fucoxanthin, 19′-hexanoyloxyfucoxanthin, and 19′butanoyloxyfucoxanthin, and photoprotective carotenoids (PPC) include violaxanthin, alloxanthin, zeaxanthin, lutein, $\alpha + \beta$ carotenes, Dd, and Dt. Dd and Dt were additionally included in the statistical analysis, hereafter referred to as Dd and Dt, respectively.

Phytoplankton absorption measurements

Absorbance samples were collected every 2–4 h as per the HPLC samples, with the total particulate absorbance (a_p) determined by the quantitative filter technique, following the IOCCG best practice protocols (IOCCG Protocol Series, 2018), using a Shimadzu UV-2501 PC spectrophotometer (ISR-2200 integrating sphere). An iterative best-fit approach of Bricaud and Stramski (1990) was used to derive the detrital absorbance (a_d) for all stations. Phytoplankton-specific absorption was calculated from the absorbance data using Eq. 2, where λ denotes wavelength, OD_f (λ) is the blank corrected optical density of the sample filter (absorbance; normalized to infrared wavelengths), V is the volume of the sample filtered (m^3), A is the effective (sample) area of the filter (m^2), and β_1 and β_2 are the coefficients for the pathlength amplification accounting for scattering through the filter (Stramski et al. 2015).

$$a(\lambda) = \ln(10)\,\beta_1\,\mathrm{OD}_f(\lambda)^{\beta_2}/(V/A). \quad (2)$$

A quality control check was applied to the absorption data, using the $a_{ph}(440) : a_{ph}(675)$ ratio, with data falling outside of 1–4 being excluded (Roesler et al. 1989; Bricaud and Stramski 1990; Sosik and Mitchell 1995; Neukermans et al. 2016).

Light history

Photosynthetically active radiation (PAR, 400–700 nm) was continuously recorded onboard through a Biospherical 2π PAR sensor attached to the ship's mast. Instantaneous surface PAR (E_0, μmol photons m^{-2} s^{-1}) at the time of sample measurement was recorded, as well as the cumulative PAR, which was binned over various time windows preceding the sample measurement (20 min, 1 h, 6 h, 12 h, and 24 h; hereafter referred to as ΣPAR20m, ΣPAR1h, ΣPAR6h, ΣPAR12h, and ΣPAR24h). Daily integrated downwelling irradiance (E_d, mol photons m^{-2} d^{-1}) for each measurement was determined from collocated GlobColour PAR 4 km monthly products.

Macronutrients

Macronutrient samples were collected directly from the ship's scientific seawater supply and stored at −20°C until analysis on land. Nitrate and silicate were measured using a Lachat Flow Injection Analyzer as previously described (Wolters 2002; Egan 2008), while phosphate was determined manually by the colorimetric method as specified by Grasshoff et al. (1983).

Statistical analysis

K-means clustering was used to group the Φ_F (λ) data into similar groupings using two different approaches: the first included all data and the second excluded the data that dictated the first cluster results (i.e., the high variance from Φ_F [λ570] and Φ_F [λ590]). Empirical orthogonal function (EOF) analysis was used to assess the variance of Φ_F (λ) spectral structure within the dataset. Intracluster Φ_F (λ) spectra were separated into a set of geometrically independent (orthogonal) modes of oscillation, which represent all the variance in the data (Craig et al. 2012). The modes, generated by computation of the eigenvectors of the covariance matrix of the dataset, were selected to be different from each other and to account for as much variance as possible. The first mode captured the largest portion of total variance and subsequent modes captured progressively less. The first three modes were used for analysis of the Φ_F (λ) dataset. All data were non-normally distributed (Shapiro–Wilk test), necessitating the use of Spearman's rho (r_s) to investigate statistical significance. All data

were standardized using the Python Scikit-learn package (Pedregosa et al. 2011) and all statistical analyses, including the EOF analysis and correlation matrices were performed using the Python SciPy library (Virtanen et al. 2020). Additional statistical tests included the student's *t*-test to examine significant differences between cruises and clusters, reported at the 95% confidence level.

Results

The data presented here cover the full latitudinal extent of the Southern Ocean from 37.03°S to 68.59°S, from the subtropical zone to the Antarctic continental shelf region, with 23 measurements from the winter cruise and 54 measurements from the summer cruise following the quality control procedures outlined in the methods. Sea surface temperatures (SST) ranged from a minimum of −1.6°C at 57°S in winter to a maximum of 21.1°C at 37°S in summer (Supporting Information Fig. S1a). Mean temperatures were substantially higher during summer (5.0°C ± 6.0°C) when compared to winter (1.1°C ± 2.3°C). Seasonal differences in the in situ light environment were even more stark and ranged from a minimum mean of instantaneous PAR (E_0; Supporting Information Fig. S4b) of 32.85 ± 92.92 μmol photons m^{-2} s^{-1} during winter to a maximum mean of 427.88 ± 483.35 μmol photons m^{-2} s^{-1} during summer, with eight measurements conducted at night during local sunset to sunrise. Daily integrated mean PAR (E_d; Supporting Information Fig. S4c) followed similar cruise patterns with a minimum mean during winter of 8.4 ± 1.2 mol photons m^{-2} d^{-1} and maximum mean during summer that was four times higher at 36.1 ± 8.0 mol photons m^{-2} d^{-1}. The only light related parameter that showed any evidence of latitudinal variability was E_d that increased from a min at the most southerly latitude to a max at the most northerly latitude. Mean Chl *a* concentrations (mg m^{-3}; Supporting Information Fig. S2a) ranged from a minimum during winter of 0.20 ± 0.06 to a maximum of 0.65 ± 0.30 during summer, while the ranges per cruises were 0.13–0.40 and 0.25–1.36 mg m^{-3} for winter and summer, respectively. Mean macronutrient concentrations for nitrate (Supporting Information Fig. S2b; μM), phosphate (Supporting Information Fig. S2c; μM) and silicate (Supporting Information Fig. S2d; μM) had more overlap with a slightly extended range of maximum and minimum in summer reflecting greater variability.

The community structure as determined by CHEMTAX (Supporting Information Fig. S3a) showed it was typically dominated by diatoms and haptophytes, but with a larger presence of prasinophytes observed in winter. In summer, the total Chl *a* was dominated (84%) by diatoms (46%) and haptophytes (38%), whereas during winter although the community was still dominated (52%) by diatoms (21%) and haptophytes (31%), there was a substantial contribution from prasinophytes (18%) and more evidence of cryptophytes and *Synechococcus*. The spatial variability of the community structure maintains the same dominance of either diatoms or haptophytes (Supporting Information Fig. S3b), with a typical increase in diversity (i.e., increasing contributions of prasinophytes, chlorophytes, cryptophytes, and *Synechococcus*) with decreasing latitude. Further examination of the community structure revealed that summer was characterized by more microphytoplankton (Supporting Information Fig. S4a; f_{micro} mean ± stdev = 0.60 ± 0.21) than nanophytoplankton (Supporting Information Fig. S4b; f_{nano} = 0.38 ± 0.19), whereas in winter these two size classes were more evenly balanced (f_{micro} = 0.47 ± 0.17 and f_{nano} = 0.52 ± 0.15). Both cruises had similar proportions of picophytoplankton (Supporting Information Fig. S4c), 0.02 ± 0.05 and 0.01 ± 0.02 for winter and summer, respectively. Some spatial variability in community structure was similarly evidence (Supporting Information Fig. S4d), with f_{pico} being present at the lower latitude stations only, with f_{nano} dominating to 55°S where it switched to being f_{micro} dominated southwards of 55°S.

Examination of the pigments showed different patterns in both the PSC (Supporting Information Fig. S5a) and PPC for the different cruises. Although both winter and summer had similar PSC/Chl *a* (Supporting Information Fig. S5a), 0.67 ± 0.09 and 0.73 ± 0.08, and PPC/Chl *a* (Supporting Information Fig. S5b), 0.13 ± 0.06 and 0.20 ± 0.05, the mean PSC : PPC ratio (Supporting Information Fig. S5c) for winter was almost double that of summer, 5.90 ± 1.92 and 3.83 ± 0.88, respectively. Consistently across all latitudes the proportion of PSC/Chl *a* was greater than PPC/Chl *a* with neither showing much spatial variability (Supporting Information Fig. S5d); however, the PSC : PPC ratio was lowest at the low latitudes and peaked at 55°S. The mean of Dd + Dt (Supporting Information Fig. S6a) was also an order of magnitude higher in summer, 0.100 ± 0.061, compared to winter, 0.012 ± 0.004; however, the mean ratio of Dt/(Dd + Dt) was similar between both summer and winter (Supporting Information Fig. S6b), 0.092 ± 0.052 and 0.068 ± 0.048, respectively. Unlike the other pigments, both Dd + Dt and Dt/(Dd + Dt) did show a strong latitudinal gradient (Supporting Information Fig. S6c) with the highest values found at high latitudes and the lowest values found at low latitudes.

The raw MFL measurements were much higher during summer than in winter (Supporting Information Fig. S7), both seasons displayed higher fluorescence values in the blue part of the spectrum at 435 nm (particularly in summer; Supporting Information Fig. S7b), indicative of the Chl *a* Soret absorption wavebands. If we normalize to Chl *a*, to account for biomass driven increases in the fluorescence signal, then seasonal disparity is substantially reduced but with fluorescence/Chl *a* (F/Chl) values in winter (Supporting Information Fig. S7c) that on average remain lower than those of summer (Supporting Information Fig. S7d), with a much lower range of maximum extent and no obvious spatial variability. Φ_F displayed very little variability between winter and summer at

375 and 505 nm (Fig. 2a–f), with similar cruises means but a large range of variability in summer (Table 1). Statistical comparisons found that on average only Φ_F (λ420) was significantly higher (*t*-test, p <0.05, df = 25) during summer when compared to winter, with summer also expressing a larger range of variability at all wavelengths. The green/orange wavebands (525–590 nm; Fig. 2g–i) showed the greatest degree of interseasonal and intraseasonal variability (though typically higher in winter). This split between the blue wavebands (375–505 nm) and the green/orange wavebands (525–590 nm) was also evident spatially (Supporting Information Fig. S8), with the blue wavebands decreasing from maximum values at the high latitudes, whereas the green/orange wavebands all peaked at 50°S.

The *K*-means clustering was performed using two different starting points, the first included all the data, which separated the Φ_F data into two clusters based upon the unique features of the green/orange wavebands (Supporting Information Fig. S9). This clustering generated significant differences at these wavebands (525–590 nm), as well as Chl *a*, f_{micro}, f_{nano}, and Dd + Dt (*t*-test, $p < 0.05$, df = 75). A second clustering was performed removing the drivers of the first clustering (i.e., Φ_F [λ570] and Φ_F [λ590]). This starting point generated two clusters that separated out by amplitude in Φ_F across all wavelengths, which were significantly different from each other (*t*-test, $p < 0.05$, df = 75). These two clusters had significant different in light (namely: E_0, E_d, ΣPAR20m, ΣPAR1h, ΣPAR6h), Dt/(Dd + Dt) and F/Chl. Although the *K*-means clustering reveals certain patterns of drivers of either the spectral shape or magnitude, it does not allow these differences (in shape and amplitude) to be investigated together, whereas an EOF analysis is able to simultaneously investigate across all modes of variability.

Table 1. Mean ± standard deviations of $\Phi_F(\lambda)$ for each MFL LED wavelength for the winter (Winter 2012) and summer (SANAE 53) cruises. The grey color indicates where there is a significant difference (*t*-test, $p < 0.05$) between winter and summer.

LED wavelength (nm)	Winter	Summer
375	0.04 ± 0.02	0.04 ± 0.02
400	0.03 ± 0.01	0.04 ± 0.02
420	0.03 ± 0.01	0.04 ± 0.02
435	0.03 ± 0.01	0.04 ± 0.02
470	0.03 ± 0.01	0.04 ± 0.02
505	0.04 ± 0.01	0.03 ± 0.02
525	0.09 ± 0.03	0.05 ± 0.02
570	0.25 ± 0.21	0.14 ± 0.10
590	0.16 ± 0.07	0.12 ± 0.08

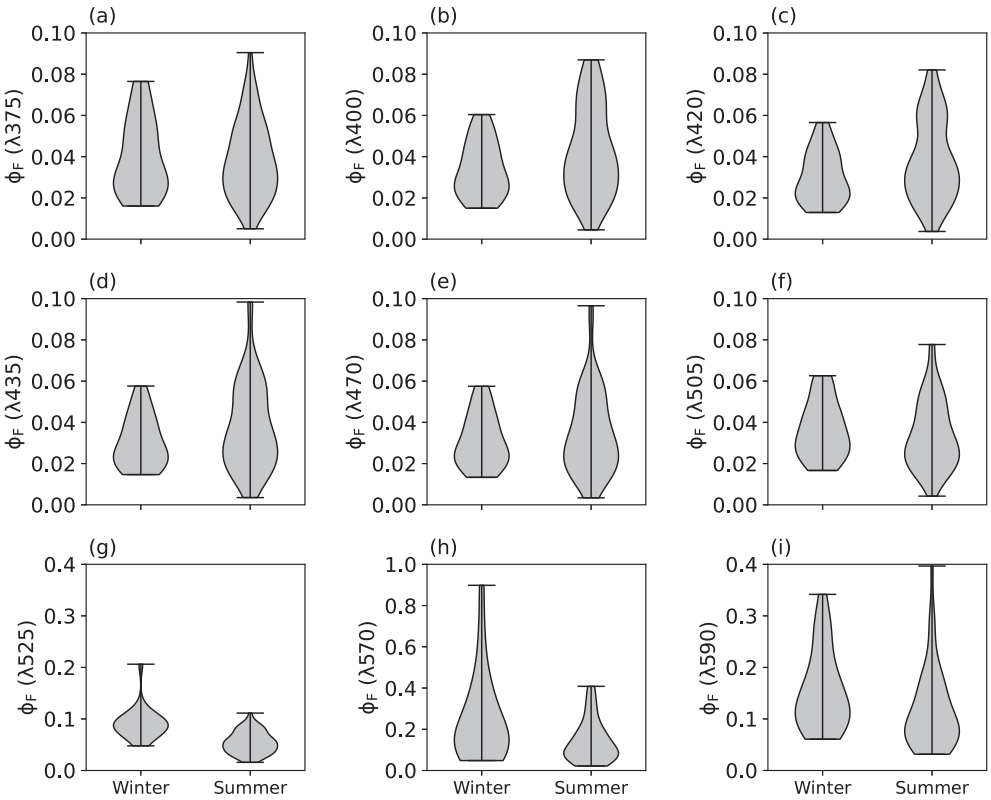

Fig. 2. Violin plots of (**a**) Φ_F (λ375), (**b**) Φ_F (λ400), (**c**) Φ_F (λ420), (**d**) Φ_F (λ435), (**e**) Φ_F (λ470), (**f**) Φ_F (λ505), (**g**) Φ_F (λ525), (**h**) Φ_F (λ570), and (**i**) Φ_F (λ590), for the winter (Winter 2012) and summer (SANAE 53) cruises.

All quality controlled Φ_F were pooled (i.e., day/night and winter/summer), with only 8 of the total 77 spectra being collected under nighttime conditions and the majority of spectra (54) coming from summer. EOF analysis on the first three modes of spectral variance found that Mode 1 described 68% of the variance, Mode 2 represented 22%, and Mode 3 5.8% (Fig. 3). Similar to the *K*-means clustering, the spectral shape of Mode 1 indicates that it is related to changes in the magnitude of Φ_F in the blue (375–505 nm) wavelengths, which is positively correlated to PSC/PPC and F/Chl, and negatively correlated to Dt(Dd + Dt), ΣPAR20m, ΣPAR1h, and ΣPAR6h (Table 2). Whereas Mode 2 exhibited an inverse spectral shape compared to that of the Φ_F spectra, with an out of phase behavior between the blue (375–470 nm) and the green/orange (525–590 nm) wavebands with the largest effect being evident on the green/orange wavebands. This mode was significantly positively correlated with the proportion of nanophytoplankton and picophytoplankton (f_{nano} and f_{pico}; Table 2), but there were 11 significant negative correlations including Chl *a*, PSC/Chl *a*, Dd + Dt, f_{micro}, the diatom/haptophyte ratio, ΣPAR20m, ΣPAR1h, and ΣPAR24h. Mode 3, with an emphasis at 525 nm, was primarily negatively correlated to SST, Chl *a*, PSC/Chl *a*, PPC-Chl *a*, Dd + Dt, ΣPAR12h, ΣPAR24h, and F/Chl, with a slight positive correlation evident with PSC/PCC. Since the inclusion of additional potential drivers in the EOF analysis such as nutrients (nitrate, phosphate) and instantaneous and daily light (E_0 and E_d) did not result in any additional significant relationships, these drivers were subsequently excluded from further investigation.

Since the Φ_F (λ) from the blue wavebands (375–505 nm) were fairly well constrained when compared to the greater variability of the green/orange wavebands (525–590 nm), an individual waveband from each of these groups was selected to examine the significant drivers using correlation matrices. These were Φ_F (λ420), as there was a significant difference between winter and summer, and Φ_F (λ570) as this waveband had the largest range of all Φ_F (λ). To reduce the number of potential drivers, we limited the analysis to only those which had shown any significance from the EOF analysis. The correlation matrices identified some similarities with the EOF and *K*-means clustering with short-term light history (ΣPAR20m and ΣPAR1h) being significantly negatively correlated with both Φ_F (λ420) and Φ_F (λ570) (Fig. 4), while neither showing any significant correlations with longer-term light history. The influence of community structure was evident in the significant positive relationship between Φ_F (λ420) and f_{micro} and

Table 2. Spearman's rho correlation coefficients for the potential drivers of the EOF spectral variance in Φ_F (λ) reported at the 95% (*) and 99% (**) level.

Driver	Mode 1	Mode 2	Mode 3
SST	−0.030	−0.057	−0.243*
[Chl *a*]	−0.069	−0.774**	−0.277*
PSC/Chl *a*	0.145	−0.251*	−0.297**
PPC/Chl *a*	−0.213	−0.201	−0.343**
PSC/PPC	0.265*	0.082	0.296**
Dd + Dt	−0.004	−0.718**	−0.314**
Dt(Dd + Dt)	−0.377**	−0.221	−0.015
f_{micro}	0.181	−0.493**	−0.025
f_{nano}	−0.138	0.283**	−0.062
f_{pico}	−0.130	0.521**	0.025
Diatom/haptophyte	0.144	−0.227*	−0.067
ΣPAR20m	−0.437**	−0.279*	−0.069
ΣPAR1h	−0.477**	−0.249*	−0.039
ΣPAR6h	−0.261*	−0.217	−0.205
ΣPAR12h	−0.013	−0.218	−0.323**
ΣPAR24h	−0.145	−0.414**	−0.407**
F/Chl	0.878**	−0.059	−0.306**

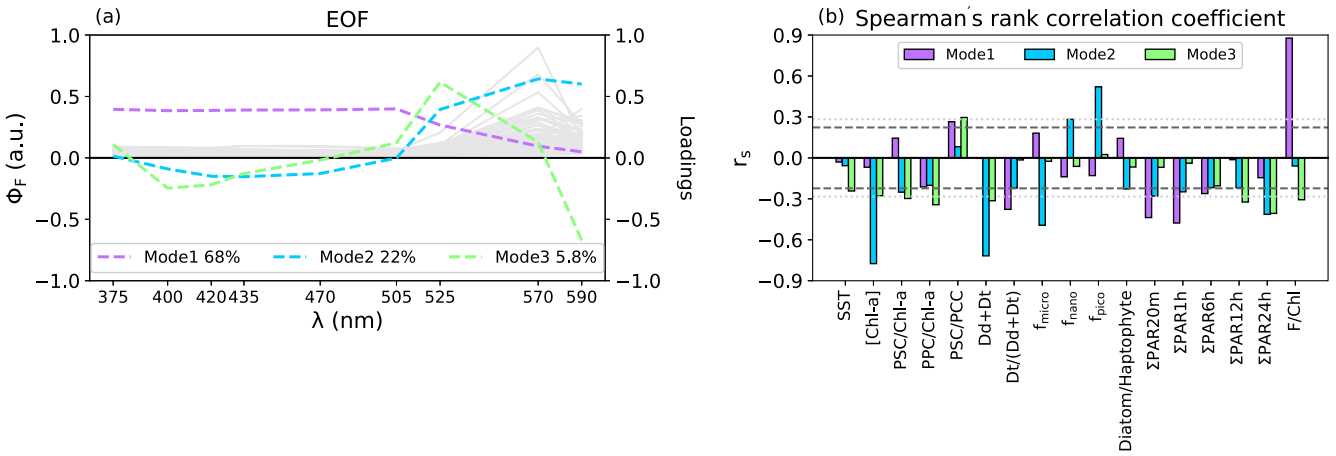

Fig. 3. EOF analysis of Φ_F (λ). (**a**) The grey Φ_F (λ) spectra plotted on the left are overlaid with the top three modes of the analysis. (**b**) The correlation coefficients (Spearman's rho [r_s]), calculated between the EOF amplitude factors and a selection of possible drivers of Φ_F (λ) variability. The dashed, grey horizontal lines represent the 95% confidence level, and the dotted grey lines represent the 99% confidence level.

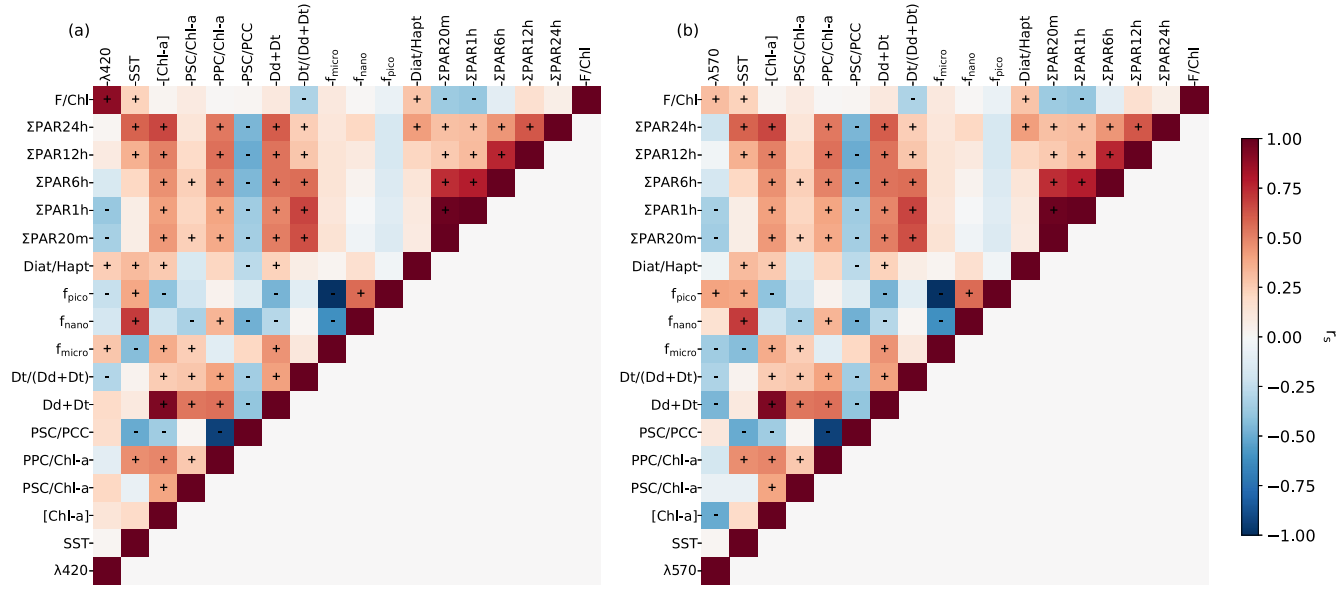

Fig. 4. Spearman's rho (r_s) correlation matrix of (**a**) Φ_F (λ420) and (**b**) Φ_F (λ570) against significant drivers (where Diat/Hapt refers to the diatom to haptophyte ratio) identified from the EOF analysis. "+" indicates significant positive ($p < 0.05$) correlations and "−" indicates significant negative ($p < 0.05$) correlations.

significantly negative relationship with f_{pico}, whereas for Φ_F (λ570) the opposite relationship with community size was true. The positive correlation between Φ_F (λ420) and f_{micro} is corroborated by a significant positive correlation with the diatom/haptophyte ratio, that is, as the community becomes more dominated by diatoms (i.e., larger cells) the Φ_F (λ420) increases. Finally, Dd + Dt, showed significant negative relationships with Φ_F (λ570), while both Φ_F (λ420) and Φ_F (λ570) showed a significant negative relationship with Dt/(Dd + Dt).

Discussion

Although phytoplankton absorption and fluorescence can provide valuable insights into photophysiology, nutrient status, and light stress, Φ_F can serve as a more valuable ecological proxy for investigating physiological responses to environmental conditions as it provides a more holistic view by integrating across both absorption and fluorescence. Indeed, the use of SICF to derive Φ_{Sat} for investigating physiological responses to environmental conditions is well established (Huot et al. 2005; Behrenfeld et al. 2009; Browning et al. 2014); however, the accurate retrieval of the SICF signal and the physiological interpretation of this signal has so far limited the application of this approach across aquatic ecosystems (Schuback et al. 2021). The physiological interpretation is particularly hampered by the limited number of in situ studies. This is likely due to the lack of dedicated instrumentation that can simultaneously measure absorption together with the incident and returning light levels required to determine in situ Φ_F. In this study, separate measurements of phytoplankton absorption and wavelength-specific fluorescence were measured, before deriving wavelength-specific Φ_F (λ) using the calibration constants from Griffith et al. (2018). The variability of Φ_F (λ) was then investigated against potential in situ drivers across a range of latitudes and two separate seasons in the Southern Ocean, the austral winter of 2012 and summer of 2013. The range of variability in the driver parameters highlights that in situ conditions spanned several different community compositions (Supporting Information Fig. S3), phytoplankton size classes (Supporting Information Fig. S4), nutrient concentrations (Supporting Information Fig. S2) as well as instantaneous and daily averaged light environments (Supporting Information Fig. S1).

The higher raw fluorescence data values in summer compared to winter (Supporting Information Fig. S8) are consistent with seasonal light limitation in the Southern Ocean in winter driven by a low zenith angle and deep mixed layers, with bloom conditions coinciding with a shoaling of the mixed layer in summer (Boyd 2002; Thomalla et al. 2011). This influence of light on raw fluorescence becomes even more apparent when we look at the diel cycle across the seasons. By averaging both the raw fluorescence data (λ420) (Supporting Information Fig. S10a) and measured E_0 (Supporting Information Fig. S10b) on both cruises, we can see that while there is a strong diel cycle in raw fluorescence data (λ420) in summer, this signal is absent in winter, despite a diel cycle being evident (albeit reduced) in E_0. This highlights the importance of both day length and amplitude in driving a higher cumulative photon dose whose impact is seen in the diurnal signal of raw fluorescence.

Another seasonal driver that is expected to regulate Southern Ocean phytoplankton productivity is that of iron

(Tagliabue et al. 2014; Ryan-Keogh et al. 2018; Mtshali et al. 2019). Previous studies have conclusively shown that an increase in the F/Chl ratio is indicative of decreased efficiency in energy transfer for photosynthesis under low iron conditions (Schallenberg et al. 2020) and reflects an increase in non-photochemical quenching. To quote Schrader et al. (2011) "This response is so universal and readily observed that it has served as the defining physiological diagnostic of iron stress in the field." Indeed, the F/Chl ratios in summer were substantially higher than those observed in winter (Supporting Information Fig. S8c,d) and indicative of iron stress, with no obvious patterns of spatial variability. Moreover, other studies have demonstrated that potentially iron limited regions have longer fluorescence lifetimes (in combination with lower photosynthesis efficiency), such as the Amundsen Sea (Park et al. 2017) and the West Antarctic Peninsula (Sherman et al. 2020).

Although all samples were dark acclimated prior to sampling during the transit from the ships intake to the instrument, it is recognized that qN-relaxation is more effective under low light conditions (Schuback et al. 2021) and that the degree of qN-relaxation will depend on a number of factors (namely acclimation time, temperature and community structure). As such, some of the variability in Φ_F is expected to be driven by variability in the degree of relaxation achieved during dark acclimation. As care was taken to maintain a constant flow rate, it is anticipated that any remaining impact of qN on Φ_F would results from variability in temperature and taxon-specific quenching mechanisms, both of which are included in the driver analysis through the inclusion of SST and pigment ratios (Dt/[Dd + Dt] and PSC : PPC).

It is worth noting that all the blue range Φ_F values fall into an acceptable range, that from previous studies (Babin et al. 1996; Letelier et al. 1997; Maritorena et al. 2000; Morrison 2003; Westberry and Siegel 2003; Huot et al. 2005; Schallenberg et al. 2008; Behrenfeld et al. 2009; Morrison and Goodwin 2010; Ostrowska 2012; Westberry et al. 2013; Browning et al. 2014; Lin et al. 2016) is considered acceptable (0.001–0.15; Supporting Information Table S1). Whereas for the green/orange range, 44% of the Φ_F (λ570) and 31% of the Φ_F (λ590) measurements fall above this suggested upper limit. The reasons for this could either be environmental conditions, sampling errors, or a combination of both. One such potential error could be the influence of Raman scattering of water, which displays an excitation peak at 550 nm (Maritorena et al. 2000; Morrison 2003). Any scattering of light, both elastic and inelastic, will redirect incident photons into the upwelling light stream (Mobley 1994). Inelastic scattering includes Chl *a* fluorescence and Raman scattering, and therefore must be quantified alongside elastic scattering of ambient solar radiation when quantifying the upwelling radiance from fluorescence. Since Raman scattering was not accounted for in this study, it could explain the potentially anomalously high Φ_F values at 570 and 590 nm. Higher Φ_F values in the green/orange spectrum (525–590 nm) as were evident in our winter measurements, has been seen before in previous studies. For example, Ostrowska (2011), showed Φ_F higher values between 470 and 610 nm across both oligotrophic and eutrophic regions; however, they offered no insight into the possible causes of this observation and suggests that this interesting feature requires further investigation.

The primary hypothesis of this study was that seasonality would emerge as the dominant driver of variability in Φ_F. However, when a *K*-means clustering approach was applied to all of the data it did not split statistically into seasons (Supporting Information Fig. S9). Instead, the clusters were based upon spectral shape with a particular focus on the high Φ_F in the green/orange wavebands. Examination of the potential drivers within these clusters found that community structure and specific pigments were significantly different. The second *K*-means clustering (excluding the green/orange wavebands) again, did not explicitly separate out into seasons but instead into clusters with characteristically high or low Φ_F in the blue wavebands. These clusters were found to have significant differences in light history and F/Chl.

Variability in the spectral shape and amplitude, as assessed by EOF, similarly identified two dominant modes of variability, with Mode 1 focused on the magnitude of Φ_F, while Mode 2 focused on the differences in spectral shape at the green/orange wavebands (525–590 nm). However, unlike the cluster analysis these results found that light history played a significant role across all modes of variability (Fig. 3; Table 2). Specifically, amplitude appears to be driven by short-term light history whereas differences in the spectral shape appear to be impacted more by long-term light history. Looking at the potential influence of light history on the magnitude of Φ_F (λ420) and Φ_F (λ570) (selected to represent the amplitude and shape characteristics of the spectra respectively), shows that both wavelengths are negatively correlated with short-term light variability. The higher Φ_F (λ570) observed in winter is possibly due to lower E_0 (Supporting Information Fig. S1b) and E_d (Supporting Information Fig. S1c), whereas in summer, qP will likely reduce Φ_F in favor of photochemistry. As the measurements in summer are unlikely to be light limited, as evidenced by the higher E_0 and E_d, the cause of a lower Φ_F (λ570) may instead be due to photoinhibition.

Another possible cause of variability in the amplitude of Φ_F could be iron limitation (Behrenfeld et al. 2009; Browning et al. 2014), with $\sim$ 57% of the summer stations being sampled in nitrate replete waters (> 10 μM; Supporting Information Fig. S2b) and relatively low biomass (< 0.5 mg m^{-3}). Although the influence of iron limitation on photophysiology in Southern Ocean phytoplankton is well established, that is, driving an increase in Φ_F under low iron conditions (Lin et al. 2016; Strzepek et al. 2019), we are unable to directly attribute the role of iron without concomitant measurements of an in situ iron concentrations. However, the role of iron is implied by the higher F/Chl ratios in summer compared to

winter, which are indicative of probable iron limitation (Park et al. 2017; Sherman et al. 2020). This is further evident in the stronger relationship between F/Chl and Φ_F (λ420) in comparison to Φ_F (λ570) (Fig. 4). No significant relationships were found with macronutrients, which is not surprising given that they were replete and thus unlikely to directly influence Φ_F. It is, however, recognized that macronutrients may play a secondary role, by impacting community structure. For example, silicate concentrations may influence the relative abundance of diatoms, which in turn will influence Φ_F through the XC.

Community structure and pigment abundances, which vary both seasonally and spatially (Supporting Information Figs. S3–S6), emerged as the dominant drivers of distinctive spectral shapes in the green/orange wavebands. For example, one of the dominant signals in Mode 2 of the EOF analysis came from the relative proportions of f_{micro}, f_{nano}, and f_{pico}, which showed a shift with decreasing cell size from a significantly positive relationship with f_{micro} to a significantly negative relationship with f_{pico}. The influence of phytoplankton size was also evident in relationships with both Φ_F (λ420) and Φ_F (λ570), with f_{micro} potentially driving an increase in Φ_F (λ420) and f_{pico} potentially driving an increase in Φ_F (λ570). This increase in Φ_F (λ570) could be driven by phycoerythrin, which absorbs strongly in the green-orange part of the spectrum (Ting et al. 2002). This phycobiliprotein is typically found in cyanobacteria (Stadnichuk et al. 2015) and cryptophytes (Doust et al. 2004, 2006), both of which are considered small phytoplankton groups that are known to occupy various Southern Ocean provinces throughout the year (Garibotti et al. 2005; Gibberd et al. 2013; Mendes et al. 2013). Indeed, the five stations with the greatest proportion of the cyanobacterium *Synechococcus* (20–28%) had some of the highest Φ_F (λ590) values (0.06–0.34). However, this same relationship was not evident for stations that had the highest abundance of cryptophytes.

Bulk phytoplankton pigment concentrations identified both PSC/Chl *a* and Dd + Dt as additional drivers of variability in the spectral shape. This is not surprising given the absorption peaks of different photosynthetic carotenoids, where, for example, phycoerythrin absorbs strongly in the green/orange region but fucoxanthin absorbs strongly in the blue region. In addition, previous studies have reported that an increase in qN capacity is driven predominantly by an increase in the size of the Dd and Dt pool size (van de Poll et al. 2005; Ragni et al. 2008). Indeed, a significant negative relationship is observed between Dd + Dt and Φ_F (λ570), but the significant positive relationship with Φ_F (λ420) contradicts this theory. As Dd is rapidly de-epoxidized to Dt on the timescale of seconds to minutes under high light exposure, it is Dt that is believed to have the fluorescence quenching effect more so than Dd (Olaizola et al. 1994). The rapid timescale of the XC and associated potential errors that may manifest in pigment sampling errors must thus be considered to avoid over interpreting Dd results. Nonetheless, the significant negative relationships observed between Dt/(Dd + Dt) and both Φ_F (λ420) and Φ_F (λ570) (Fig. 4), and the large positive and negative r_s values of Dd + Dt for Mode 2 of the EOF analysis (Fig. 3b), suggest that low concentrations of photoprotective pigments and low qN activity results in high Φ_F, which agrees with the findings of previous studies (Maritorena et al. 2000; Morrison 2003).

Although single wavelength Φ_F instruments have been previously deployed in the Southern Ocean (Park et al. 2017; Sherman et al. 2020), this study is the first to present wavelength-specific Φ_F that has been derived using an instrument specific calibration. This study has demonstrated that the amplitude of Φ_F is predominantly driven by both light history, with high light being associated with reduced Φ_F, and potential iron limitation (i.e., F/Chl), associated with higher Φ_F in the blue region. Both of these drivers show strong seasonal differences, with no clear spatial patterns. The spectral shape of Φ_F, on the other hand, is predominantly driven by community composition and bulk pigment concentrations, with smaller phycoerythrin containing phytoplankton driving higher Φ_F in the green/orange region. These drivers of spectral shape not only vary seasonally, but also show strong spatial patterns that appear to be centered around 50–55°S. As such, although the spectra of Φ_F did not cluster out seasonally, seasonality remains a dominant driver of Φ_F by impacting the drivers of variability in both amplitude and spectral shape, with latitudinal variability emerging as a driver of variability community aspects that influence the spectral shape. With confidence in the derivation of these UW Φ_F values, in addition to a fairly broad understanding of their drivers, the knowledge gained here can be used in conjunction with remote sensing-based methods to investigate long-term spatially resolved changes in Southern Ocean phytoplankton photosynthetic efficiency.

Data availability statement

All data can be found online at Zenodo (DOI: 10.5281/zenodo.7330550). GlobColour data (http://globcolour.info) used in this study has been developed, validated, and distributed by ACRI-ST, France.

References

Abbott, M. R., J. G. Richman, J. S. Nahorniak, and B. S. Barksdale. 2001. Meanders in the Antarctic Polar Frontal Zone and their impact on phytoplankton. Deep Sea Res. Part II Topic. Stud. Oceanogr. **48**: 3891–3912. doi:10.1016/S0967-0645(01)00073-X

Babin, M., A. Morel, and B. Gentili. 1996. Remote sensing of sea surface Sun-induced chlorophyll fluorescence: consequences of natural variations in the optical characteristics of phytoplankton and the quantum yield of chlorophyll a fluorescence. Int. J. Remote Sens. **17**: 2417–2448. doi:10.1080/01431169608948781

Behrenfeld, M. J., and others. 2009. Satellite-detected fluorescence reveals global physiology of ocean phytoplankton. Biogeosciences **6**: 779–794. doi:10.5194/bg-6-779-2009

Beutler, M., K. H. Wiltshire, B. Meyer, C. Moldaenke, and H. Dau. 1998. Rapid depth-profiling of the distribution of spectral groups of microalgae in lakes, rivers and in the sea, p. 4301–4304. *In* G. Garab [ed.], Photosynthesis: Mechanisms and effects, Kluwer Academic Publishers.

Beutler, M., K. H. Wiltshire, B. Meyer, C. Moldaenke, C. Lüring, M. Meyerhöfer, U.-P. Hansen, and H. Dau. 2002. A fluorometric method for the differentiation of algal populations in vivo and in situ. Photosyn. Res. **72**: 39–53. doi:10.1023/A:1016026607048

Beutler, M., K. H. Wiltshire, M. Arp, J. Kruse, C. Reineke, C. Moldaenke, and U.-P. Hansen. 2003. A reduced model of the fluorescence from the cyanobacterial photosynthetic apparatus designed for the in situ detection of cyanobacteria. Biochim. Biophys. Acta Bioenerg. **1604**: 33–46. doi:10.1016/S0005-2728(03)00022-7

Boyd, P. W. 2002. Environmental factors controlling phytoplankton processes in the Southern Ocean. J. Phycol. **38**: 844–861. doi:10.1046/j.1529-8817.2002.t01-1-01203.x

Bricaud, A., and D. Stramski. 1990. Spectral absorption coefficients of living phytoplankton and nonalgal biogenous matter: A comparison between the Peru upwelling area and the Sargasso Sea. Limnol. Oceanogr. **35**: 562–582. doi:10.4319/lo.1990.35.3.0562

Browning, T. J., H. A. Bouman, and C. M. Moore. 2014. Satellite detected fluorescence: Decoupling nonphotochemical quenching form iron stress signals in the South Atlantic and Southern Ocean. Global Biogeochem. Cycl. **28**: 510–524. doi:10.1002/2013GB004773

Brunet, C., G. Johnsen, J. Lavaud, and S. Roy. 2011. Pigments and photoacclimation processes, p. 445–471. *In* C. A. Llewellyn, E. S. Egeland, G. Johnsen, and S. Roy [eds.], Phytoplankton pigments: Characterization, chemotaxonomy and applications in oceanography. Cambridge University Press.

Cowles, T. J., R. A. Desiderio, and S. Neuer. 1993. In situ characterization of phytoplankton from vertical profiles of fluorescence emission spectra. Mar. Biol. **115**: 217–222. doi:10.1007/BF00346338

Craig, S. E., C. T. Jones, W. K. W. Li, G. Lazin, E. Horne, C. Caverhill, and J. J. Cullen. 2012. Deriving optical metrics of coastal phytoplankton biomass from ocean colour. Remote Sens. Environ. **119**: 72–83. doi:10.1016/j.rse.2011.12.007

Demers, S., S. Roy, R. Gagnon, and C. Vignault. 1991. Rapid light-induced changes in cell fluorescence and in xanthophyll-cycle pigments of *Alexandrium excavatum* (Dinophyceae) and *Thalassiosira pseudonana* (Bacillariophyceae): A photoprotection mechanism. Mar. Ecol. Prog. Ser. **76**: 185–193.

Demmig-Adams, B. 1990. Carotenoids and photoprotection in plants: A role for the xanthophyll zeaxanthin. Biochim. Biophys. Acta Bioenerg. **1020**: 1–24. doi:10.1016/0005-2728(90)90088-L

Doust, A. B., C. N. J. Marai, S. J. Harrop, K. E. Wilk, P. M. G. Curmi, and G. D. Scholes. 2004. Developing a structure–function model for the cryptophyte phycoerythrin 545 using ultrahigh resolution crystallography and ultrafast laser spectroscopy. J. Mol. Biol. **344**: 135–153. doi:10.1016/j.jmb.2004.09.044

Doust, A. B., K. E. Wilk, P. M. G. Curmi, and G. D. Scholes. 2006. The photophysics of cryptophyte light-harvesting. J. Photochem. Photobiol. A Chem. **184**: 1–17. doi:10.1016/j.jphotochem.2006.06.006

Egan, L. 2008. QuickChem method 31–107-04-1-C—Nitrate and/or nitrite in brackish or seawater. Lachat Instruments.

Garibotti, I. A., M. Vernet, and M. E. Ferrario. 2005. Annually recurrent phytoplanktonic assemblages during summer in the seasonal ice zone west of the Antarctic Peninsula (Southern Ocean). Deep Sea Res. Part I Oceanogr. Res. Pap. **52**: 1823–1841. doi:10.1016/j.dsr.2005.05.003

Gibberd, M. J., E. Kean, R. Barlow, S. Thomalla, and M. Lucas. 2013. Phytoplankton chemotaxonomy in the Atlantic sector of the Southern Ocean during late summer 2009. Deep Sea Res. Part I Oceanogr. Res. Pap. **78**: 70–78. doi:10.1016/j.dsr.2013.04.007

Grasshoff, K., M. Ehrhardt, and K. Kremling. 1983. Methods of seawater analysis, 419 p, 2nd ed. Verlag Chemie Weinhein.

Greene, R. M., R. J. Geider, and P. G. Falkowski. 1991. Effect of iron limitation on photosynthesis in a marine diatom. Limnol. Oceanogr. **36**: 1772–1782. doi:10.4319/lo.1991.36.8.1772

Griffith, D. J., E. L. Bone, S. J. Thomalla, and S. Bernard. 2018. Calibration of an in-water multi-excitation fluorometer for the measurement of phytoplankton chlorophyll-a fluorescence quantum yield. Opt. Express **26**: 18863. doi:10.1364/OE.26.018863

Horton, P., and A. Ruban. 2005. Molecular design of the photosystem II light-harvesting antenna: photosynthesis and photoprotection. J. Exp. Bot. **56**: 365–373. doi:10.1093/jxb/eri023

Huot, Y., C. A. Brown, and J. J. Cullen. 2005. New algorithms for MODIS sun-induced chlorophyll fluorescence and a comparison with present data products. Limnol. Oceanogr. Methods **3**: 108–130. doi:10.4319/lom.2005.3.108

Johnsen, G., B. B. Prézelin, and R. V. M. Jovine. 1997. Fluorescence excitation spectra and light utilization in two red tide dinoflagellates. Limnol. Oceanogr. **42**: 1166–1177. doi:10.4319/lo.1997.42.5_part_2.1166

Kiefer, D. A., and R. A. Reynolds. 1992. Advances in understanding phytoplankton fluorescence and photosynthesis, p. 155–174. *In* P. G. Falkowski and A. Woodhead [eds.], Primary productivity and biogeochemical cycles in the sea. Plenum.

Krause, G. H., and E. Weis. 1991. Chlorophyll fluorescence and photosynthesis: The basics. Annu. Rev. Plant Physiol. Plant Mol. Biol. **42**: 313–349. doi:10.1146/annurev.pp.42.060191.001525

Kropuenske, L. R., M. M. Mills, G. L. van Dijken, S. Bailey, D. H. Robinson, N. A. Welschmeyer, and K. R. Arrigoa. 2009. Photophysiology in two major Southern Ocean phytoplankton taxa: Photoprotection in *Phaeocystis antarctica* and *Fragilariopsis cylindrus*. Limnol. Oceanogr. **54**: 1176–1196. doi:10.4319/lo.2009.54.4.1176

Laney, S. R., R. M. Letelier, and M. R. Abbott. 2005. Parameterizing the natural fluorescence kinetics of *Thalassiosira weissflogii*. Limnol. Oceanogr. **50**: 1499–1510. doi:10.4319/lo.2005.50.5.1499

Lavaud, J., B. Rousseau, H. J. van Gorkom, and A.-L. Etienne. 2002. Influence of the diadinoxanthin pool size on photoprotection in the marine planktonic diatom *Phaeodactylum tricornutum*. Plant Physiol. **129**: 1398–1406. doi:10.1104/pp.002014

Letelier, R. M., M. R. Abbott, and D. M. Karl. 1997. Chlorophyll natural fluorescence response to upwelling events in the Southern Ocean. Geophys. Res. Lett. **24**: 409–412. doi:10.1029/97GL00205

Lin, H., F. I. Kuzminov, J. Park, S. H. Lee, P. G. Falkowski, and M. Y. Gorbunov. 2016. Phytoplankton: The fate of photons absorbed by phytoplankton in the global ocean. Science **1979**: 264–267. doi:10.1126/science.aab2213

Macey, A. I., T. Ryan-Keogh, S. Richier, C. M. Moore, and T. S. Bibby. 2014. Photosynthetic protein stoichiometry and photophysiology in the high latitude north Atlantic. Limnol. Oceanogr. **59**: 1853–1864. doi:10.4319/lo.2014.59.6.1853

Mackey, M. D., D. J. Mackey, H. W. Higgins, and S. W. Wright. 1996. CHEMTAX—A program for estimating class abundances from chemical markers: Application to HPLC measurements of phytoplankton. Mar. Ecol. Prog. Ser. **144**: 265–283. doi:10.3354/meps144265

Maritorena, S., A. Morel, and B. Gentili. 2000. Determination of the fluorescence quantum yield by oceanic phytoplankton in their natural habitat. Appl. Opt. **39**: 6725–6737. doi:10.1364/AO.39.006725

Mendes, C. R. B., V. M. Tavano, M. C. Leal, M. S. de Souza, V. Brotas, and C. A. E. Garcia. 2013. Shifts in the dominance between diatoms and cryptophytes during three late summers in the Bransfield Strait (Antarctic Peninsula). Polar Biol. **36**: 537–547. doi:10.1007/s00300-012-1282-4

Mobley, C. M. 1994. Light and water: Radiative transfer in natural waters, 1st ed. Academic Press, p. 592.

Moisan, T. A., and M. Olaizola. 1998. Xanthophyll cycling in *Phaeocystis antarctica*: Changes in cellular fluorescence. Mar. Ecol. Prog. Ser. **169**: 113–121.

Morrison, J. R. 2003. In situ determination of the quantum yield of phytoplankton chlorophyll a fluorescence: A simple algorithm, observations, and a model. Limnol. Oceanogr. **48**: 618–631. doi:10.4319/lo.2003.48.2.0618

Morrison, J. R., and D. S. Goodwin. 2010. Phytoplankton photocompensation from space-based fluorescence measurements. Geophys. Res. Lett. **37**. doi:10.1029/2009GL041799

Mtshali, T. N., and others. 2019. Seasonal depletion of the dissolved iron reservoirs in the sub-antarctic zone of the Southern Atlantic Ocean. Geophys. Res. Lett. **46**: 4386–4395. doi:10.1029/2018GL081355

Müller, P., X.-P. Li, and K. K. Niyogi. 2001. Non-photochemical quenching. A response to excess light energy. Plant Physiol. **125**: 1558–1566. doi:10.1104/pp.125.4.1558

Neukermans, G., R. A. Reynolds, and D. Stramski. 2016. Optical classification and characterization of marine particle assemblages within the western Arctic Ocean. Limnol. Oceanogr. **61**: 1472–1494. doi:10.1002/lno.10316

Olaizola, M., J. la Roche, Z. Kolber, and P. G. Falkowski. 1994. Non-photochemical fluorescence quenching and the diadinoxanthin cycle in a marine diatom. Photosynth. Res. **41**: 357–370. doi:10.1007/BF00019413

Ostrowska, M. 2011. Ostrowska, Mirosława. Dependence between the quantum yield of chlorophyll a fluorescence in marine phytoplankton and trophicity in low irradiance level. Optic. Appl. **4**: 567–577.

Ostrowska, M. 2012. Model of the dependence of the sun-induced chlorophyll a fluorescence quantum yield on the environmental factors in the sea. Opt Express **20**: 23300–23317. doi:10.1364/OE.20.023300

Park, J., F. I. Kuzminov, B. Bailleul, E. J. Yang, S. H. Lee, P. G. Falkowski, and M. Y. Gorbunov. 2017. Light availability rather than Fe controls the magnitude of massive phytoplankton bloom in the Amundsen Sea polynyas, Antarctica. Limnol. Oceanogr. **62**: 2260–2276. doi:10.1002/lno.10565

Pedregosa, F., G. Varoquaux, and A. Gramfort. 2011. Scikit-learn: Machine learning in Python. J. Mach. Learn. Res. **85**: 2825–2830.

Ragni, M., R. L. Airs, N. Leonardos, and R. J. Geider. 2008. Photoinhibition of PSII in *Emiliani huxleyi* (Haptophyta) under high light stress: The roles of photoacclimation, photoprotection and photorepair. J. Phycol. **44**: 670–683. doi:10.1111/j.1529-8817.2008.00524.x

Ras, J., H. Claustre, and J. Uitz. 2008. Spatial variability of phytoplankton pigment distributions in the Subtropical South Pacific Ocean: Comparison between in situ and predicted data. Biogeosciences **5**: 353–369. doi:10.5194/bg-5-353-2008

Raven, J. A., M. C. Evans, and R. E. Korb. 1999. The role of trace metals in photosynthetic electron transport in O_2-evolving organisms. Photosynth. Res. **60**: 111–150.

Roesler, C. S., M. J. Perry, and K. L. Carder. 1989. Modeling in situ phytoplankton absorption from total absorption spectra in productive inland marine waters. Limnol Oceanogr **34**: 1510–1523. doi:10.4319/lo.1989.34.8.1510

Ryan-Keogh, T. J., S. J. Thomalla, T. N. Mtshali, N. R. van Horsten, and H. J. Little. 2018. Seasonal development of iron limitation in the sub-Antarctic zone. Biogeosciences **15**: 4647–4660. doi:10.5194/bg-15-4647-2018

Sathyendranath, S., and others. 2019. An ocean-colour time series for use in climate studies: The experience of the Ocean-457 Colour Climate Change Initiative (OC-CCI). Sensors **19**: 458. doi:10.3390/s19194285

Schallenberg, C., M. R. Lewis, D. E. Kelley, and J. J. Cullen. 2008. Inferred influence of nutrient availability on the relationship between Sun-induced chlorophyll fluorescence and incident irradiance in the Bering Sea. J. Geophys. Res. Oceans **113**: 1–21. doi:10.1029/2007JC004355

Schallenberg, C., R. F. Strzepek, N. Schuback, L. A. Clementson, P. W. Boyd, and T. W. Trull. 2020. Diel quenching of Southern Ocean phytoplankton fluorescence is related to iron limitation. Biogeosciences **17**: 793–812. doi:10.5194/bg-17-793-2020

Schrader, P. S., A. J. Milligan, and M. J. Behrenfeld. 2011. Surplus photosynthetic antennae complexes underlie diagnostics of iron limitation in a cyanobacterium. PLoS One **6**: e18753. doi:10.1371/journal.pone.0018753

Schuback, N., and others. 2021. Single-turnover variable chlorophyll fluorescence as a tool for assessing phytoplankton photosynthesis and primary productivity: Opportunities, caveats and recommendations. Front. Mar. Sci. **8**. doi:10.3389/fmars.2021.690607

Sherman, J., M. Y. Gorbunov, O. Schofield, and P. G. Falkowski. 2020. Photosynthetic energy conversion efficiency in the West Antarctic Peninsula. Limnol. Oceanogr. **65**: 2912–2925. doi:10.1002/lno.11562

Sosik, H. M., and B. G. Mitchell. 1995. Light absorption by phytoplankton, photosynthetic pigments and detritus in the California Current System. Deep Sea Res. Part I Oceanogr. Res. Pap. **42**: 1717–1748. doi:10.1016/0967-0637(95)00081-G

Stadnichuk, I. N., P. M. Krasilnikov, and D. v Zlenko. 2015. Cyanobacterial phycobilisomes and phycobiliproteins. Microbiology **84**: 101–111. doi:10.1134/S0026261715020150

Stramski, D., R. A. Reynolds, S. Kaczmarek, J. Uitz, and G. Zheng. 2015. Correction of pathlength amplification in the filter-pad technique for measurements of particulate absorption coefficient in the visible spectral region. Appl. Opt. **54**: 6763. doi:10.1364/AO.54.006763

Strzepek, R. F., P. W. Boyd, and W. G. Sunda. 2019. Photosynthetic adaptation to low iron, light, and temperature in Southern Ocean phytoplankton. Proc. Nat. Acad. Sci. **116**: 4388–4393. doi:10.1073/pnas.1810886116

Tagliabue, A., J. B. Sallée, A. R. Bowie, M. Lévy, S. Swart, and P. W. Boyd. 2014. Surface-water iron supplies in the Southern Ocean sustained by deep winter mixing. Nat. Geosci. **7**: 314–320. doi:10.1038/ngeo2101

Thomalla, S. J., N. Fauchereau, S. Swart, and P. M. S. Monteiro. 2011. Regional scale characteristics of the seasonal cycle of chlorophyll in the Southern Ocean. Biogeosciences **8**: 2849–2866. doi:10.5194/bg-8-2849-2011

Ting, C. S., G. Rocap, J. King, and S. W. Chisholm. 2002. Cyanobacterial photosynthesis in the oceans: the origins and significance of divergent light-harvesting strategies. Trends Microbiol. **10**: 134–142.

van de Poll, W. H., M. A. van Leeuwe, J. Roggeveld, and A. G. J. Buma. 2005. Nutrient limitation and high irradiance acclimation reduce PAR and UV-induced viability loss in the Antarctic diatom *Chaeotoceros brevis* (Bacillariophycae). J. Phycol. **41**: 840–850. doi:10.1111/j.1529-8817.2005.00105.x

Vidussi, F., H. Claustre, B. B. Manca, A. Luchetta, and J.-C. Marty. 2001. Phytoplankton pigment distribution in relation to upper thermocline circulation in the eastern Mediterranean Sea during winter. J. Geophys. Res. Oceans **106**: 19939–19956. doi:10.1029/1999JC000308

Virtanen, P., R. Gommers, and T. E. Oliphant. 2020. SciPy 1.0: Fundamental algorithms for scientific computing in Python. Nat. Methods **17**: 261–272. doi:10.1038/s41592-019-0686-2

Westberry, T. K., and D. A. Siegel. 2003. Phytoplankton natural fluorescence variability in the Sargasso Sea. Deep Sea Res. Part I Oceanogr. Res. Pap. **50**: 417–434. doi:10.1016/S0967-0637(03)00019-0

Westberry, T. K., M. J. Behrenfeld, A. J. Milligan, and S. C. Doney. 2013. Retrospective satellite ocean color analysis of purposeful and natural ocean iron fertilization. Deep Sea Res. Part I Oceanogr. Res. Pap. **73**: 1–16. doi:10.1016/j.dsr.2012.11.010

Wientjes, E., H. van Amerongen, and R. Croce. 2013. Quantum yield of charge separation in photosystem II: Functional effect of changes in the antenna size upon light acclimation. J. Phys. Chem. B **117**: 11200–11208. doi:10.1021/jp401663w

Wolters, M. 2002. Quickchem method 31–114-27-1-D—Silicate in brackish or seawater. Lachat Instruments.

Wykoff, D. D., J. P. Davies, A. Melis, and A. R. Grossman. 1998. The regulation of photosynthetic electron transport during nutrient deprivation in *Chlamydomonas reinhardtii*. Plant Physiol. **117**: 129–139. doi:10.1104/pp.117.1.129

Yoshida, M., T. Horiuchi, and Y. Nagasawa. 2011. In situ multi-excitation chlorophyll fluorometer for phytoplankton measurements: Technologies and applications beyond conventional fluorometers, Institute of Electrical and Electronics Engineers, p. 1–4. *In* OCEANS'11 MTS/IEEE KONA.

Acknowledgements

The authors would like to acknowledge the support and assistance of the captain and crew of the R/V SA Agulhas II, along with all the participants on both research cruises. T.J.R.K., E.L.B., and S.J.T. were supported through the CSIR's Southern Ocean-Carbon Climate Observatory (SOCCO) Program (http://socco.org.za) funded by the Department of Science and Innovation (DST/CON 0182/2017) and the CSIR's Parliamentary Grant. The authors would like to acknowledge the funding received from a number of grants from the National Research Foundation, South Africa, grant numbers 118751 (S.J.T.) and 110729 (S.J.T.). E.L.B. would like to acknowledge funding received from the Marine

Research Institute, University of Cape Town and the Nansen-Tutu Centre for Marine Environmental Research, University of Cape Town.

Submitted 16 March 2022
Revised 05 September 2022
Accepted 17 December 2022

Associate editor: Ilana Berman-Frank

Conflict of Interest

The authors declare no conflice of interest.